Endogenous dendritic cells from the tumor microenvironment support T-ALL growth via IGF1R activation

Todd A. Triplett[a], Kim T. Cardenas[a,1], Jessica N. Lancaster[a], Zicheng Hu[a], Hilary J. Selden[a], Guadalupe J. Jasso[a], Sadhana Balasubramanyam[a], Kathy Chan[a], LiQi Li[b], Xi Chen[c,d], Andrea N. Marcogliese[e], Utpal P. Davé[f], Paul E. Love[b], and Lauren I. R. Ehrlich[a,2]

[a]Department of Molecular Biosciences, Institute for Cellular and Molecular Biology, The University of Texas at Austin, Austin, TX 78712; [b]Section on Hematopoiesis and Lymphocyte Biology, Eunice Kennedy Shriver National Institute of Child Health and Human Development, National Institutes of Health, Bethesda, MD 20892; [c]Division of Biostatistics, Department of Health Sciences, University of Miami Miller School of Medicine, Miami, FL 33136; [d]Sylvester Comprehensive Cancer Center, University of Miami Miller School of Medicine, Miami, FL 33136; [e]Department of Pathology and Immunology, Baylor College of Medicine, Houston, TX 77030; and [f]Division of Hematology/Oncology, Tennessee Valley Healthcare System and Vanderbilt University Medical Center, Nashville, TN 37232

Edited by Zena Werb, University of California, San Francisco, CA, and approved January 14, 2016 (received for review October 15, 2015)

Primary T-cell acute lymphoblastic leukemia (T-ALL) cells require stromal-derived signals to survive. Although many studies have identified cell-intrinsic alterations in signaling pathways that promote T-ALL growth, the identity of endogenous stromal cells and their associated signals in the tumor microenvironment that support T-ALL remains unknown. By examining the thymic tumor microenvironments in multiple murine T-ALL models and primary patient samples, we discovered the emergence of prominent epithelial-free regions, enriched for proliferating tumor cells and dendritic cells (DCs). Systematic evaluation of the functional capacity of tumor-associated stromal cells revealed that myeloid cells, primarily DCs, are necessary and sufficient to support T-ALL survival ex vivo. DCs support T-ALL growth both in primary thymic tumors and at secondary tumor sites. To identify a molecular mechanism by which DCs support T-ALL growth, we first performed gene expression profiling, which revealed up-regulation of platelet-derived growth factor receptor beta (*Pdgfrb*) and insulin-like growth factor I receptor (*Igf1r*) on T-ALL cells, with concomitant expression of their ligands by tumor-associated DCs. Both *Pdgfrb* and *Igf1r* were activated in ex vivo T-ALL cells, and coculture with tumor-associated, but not normal thymic DCs, sustained IGF1R activation. Furthermore, IGF1R signaling was necessary for DC-mediated T-ALL survival. Collectively, these studies provide the first evidence that endogenous tumor-associated DCs supply signals driving T-ALL growth, and implicate tumor-associated DCs and their mitogenic signals as auspicious therapeutic targets.

T-ALL | leukemia | dendritic cell | tumor microenvironment | IGF1R

T-cell acute lymphoblastic leukemia (T-ALL) is an aggressive malignancy of T-cell progenitors that predominantly affects children and adolescents. Intensified chemotherapeutic regimens have improved 5-y event-free survival rates to over 75% in children and 50% in adults. However, these therapies are toxic, and patients who fail to respond or relapse have poor outcomes (1). The main focus of T-ALL research has been identification of cell-intrinsic genetic permutations that promote tumor growth, such as activating mutations in the transcription factor *NOTCH1*, deletion of tumor suppressor genes in the *CDKN2A* locus, and aberrant activation of transcriptional regulators such as LIM domain only 2 (*LMO2*) (1). Despite our understanding of these common cell-intrinsic alterations, we have yet to develop successful, targeted therapeutic approaches to improve patient outcomes, suggesting that we need to broaden our understanding of other factors promoting T-ALL growth (1).

Tumor progression is driven not only by cell-intrinsic alterations but also by dynamic interactions between cancer cells and the surrounding tumor microenvironment (2). For example, cancer-associated fibroblasts (CAFs) secrete factors that promote tumor survival, angiogenesis, and recruitment of inflammatory cells. CAFs also mediate tissue remodeling that promotes tumor growth and metastasis (3). Tumor-associated macrophages (TAMs), which resemble alternatively activated (M2) macrophages (4), also support tumor growth. TAMs suppress antitumor immune responses, promote tumor invasion and angiogenesis, and are negatively associated with clinical outcomes (5). Macrophage depletion slows tumor progression in multiple cancer models (6–8). Dendritic cells (DCs) within tumor microenvironments also have aberrant phenotypes and have been implicated in suppression of antitumor adaptive immune responses (9). Thus, through mitogenic signaling, tissue remodeling, and suppression of adaptive immunity, heterogeneous cells in the tumor microenvironment cooperate to promote growth of solid and hematologic malignancies (2). Importantly, human primary T-ALL samples have been shown to require stromal-derived signals for survival (10). Thus, identification of tumor stromal cell types that support T-ALL could unveil novel therapeutic targets.

There is ample reason to suspect that the thymic microenvironment, the primary site of T-ALL, contributes to lymphomagenesis.

Significance

T-cell acute lymphoblastic leukemia (T-ALL) is a malignancy of developing T cells. Cancer cell growth is often driven by cell-intrinsic alterations in signaling pathways as well as extrinsic signals from the tumor microenvironment. Here we identify tumor-associated dendritic cells as a key endogenous cell type in the tumor microenvironment that promotes murine T-ALL growth and survival at both primary and metastatic tumor sites. We also find that tumor-associated dendritic cells activate the insulin-like growth factor I receptor in T-ALL cells, which is critical for their survival. Analysis of primary patient T-ALL samples reveals phenotypically analogous tumor microenvironments. Our findings suggest that targeting signals from the tumor microenvironment could expand therapeutic options for T-ALL.

Author contributions: T.A.T., K.T.C., and L.I.R.E. designed research; T.A.T., K.T.C., J.N.L., H.J.S., G.J.J., S.B., and K.C. performed research; L.L., A.N.M., U.P.D., and P.E.L. contributed new reagents/analytic tools; T.A.T., K.T.C., J.N.L., Z.H., K.C., X.C., and L.I.R.E. analyzed data; and T.A.T. and L.I.R.E. wrote the paper.

The authors declare no conflict of interest.

This article is a PNAS Direct Submission.

Data deposition: The transcriptional profiling data reported in this paper have been deposited in the Gene Expression Omnibus (GEO) database, www.ncbi.nlm.nih.gov/geo (accession no. GSE54609).

[1]Present address: Department of Molecular Medicine, University of Texas Health Science Center at San Antonio, San Antonio, TX 78240.

[2]To whom correspondence should be addressed. Email: lehrlich@austin.utexas.edu.

This article contains supporting information online at www.pnas.org/lookup/suppl/doi:10.1073/pnas.1520245113/-/DCSupplemental.

Normal thymocytes must engage in bidirectional signaling with heterogeneous thymic stromal cells to promote proper differentiation of both thymocyte and stromal compartments (11, 12). Thymic stromal cells consist of hematopoietic cells, such as DCs and macrophages, and nonhematopoietic cells, such as thymic epithelial cells (TECs) and fibroblasts. Thymocyte:TEC crosstalk is essential at multiple stages of T-cell development. TECs express NOTCH ligands and IL-7, which are required for differentiation of normal T-cells (13–15), but have also been implicated in T-ALL tumorigenesis (10, 16). Thus, nascent lymphoma cells may coopt signals in the thymic microenvironment to promote tumor growth. Previous studies demonstrated that stromal support is required for ex vivo survival of mouse and human T-ALL cells (10, 17–20) and implicated IL-7 and NOTCH1 signaling in promoting tumor survival (10, 16–18). Together, these findings suggest that TECs might promote T-ALL. However, the above studies addressed the role of stroma in supporting T-ALL predominantly using cell lines and exogenous cytokines; thus, the contribution of endogenous stromal cells in the T-ALL tumor microenvironment remains largely unexplored.

Herein, we identify primary stromal cells from the endogenous tumor microenvironment that support T-ALL growth ex vivo. Our data reveal that DCs are expanded within primary and metastatic T-ALL tumor microenvironments. Despite the essential contribution of TECs to normal thymocyte development, TECs are dispensable for T-ALL survival in tumor:stromal cocultures. In contrast, myeloid cells, particularly DCs from tumor microenvironments at both primary and secondary tumor sites, are necessary and sufficient to support growth of T-ALL cells. Tumor-associated, but not wild-type (WT), thymic DCs support T-ALL survival and activate IGF1R and downstream mitogen-activated protein kinase (MAPK) signaling in T-ALL cells. Importantly, IGF1R activation is required for DC-mediated T-ALL survival. Analysis of primary T-ALL patient tissues reveals similar tumor microenvironments, consisting of expansive epithelial-free regions with infiltrating DCs. Together, our findings reveal an unanticipated role for endogenous tumor-associated DCs in directly promoting survival of T-ALL cells through an IGF1R-dependent mechanism, suggesting tumor-associated DCs or their corresponding mitogenic signals might serve as auspicious therapeutic targets.

Results

Primary T-ALL Cells Require Tumor Stroma for Survival ex Vivo. To investigate the contribution of tumor stroma to T-ALL growth, we used the LN3 murine model of T-ALL in which endogenous TCRαβ rearrangements promote spontaneous lymphomagenesis (21). Although the oncogenic lesions driving T-ALL in LN3 mice have not been elucidated, activation of NOTCH1 and NFAT were previously implicated (21). *Notch1* exon sequencing revealed nonsynonymous mutations in the heterodimerization or PEST domains in 64% (9/14) of primary LN3 tumors, with premature STOP codons in the PEST domains of 42% (6/14) of LN3 T-ALLs (Table S1). Thus, T-ALL in the LN3 model shares characteristics with human NOTCH-driven cortical T-ALL, including constitutive NOTCH signaling and NFAT activation (Table S1) (19, 21, 22), as well as expression of CD8 with variable levels of CD4 (21), and elevated expression of the NOTCH1 transcriptional targets *Hes1*, *Dtx1*, and *pTCRa* (https://gexc.stanford.edu/models/1118/genes). We found that 60% of LN3 mice developed T-ALL by 1 y of age (Fig. 1*A*).

To determine whether endogenous tumor stromal cells support T-ALL growth, we cultured primary LN3 T-ALL cells in the presence or absence of stroma from WT or tumor-bearing thymi. Whereas tumor cells cultured alone or with WT thymic stroma underwent cell death, T-ALL cells cultured with tumor-associated stroma survived (Fig. 1 *B* and *C*). Furthermore, a significantly higher proportion of viable T-ALL cells proliferated in the presence of tumor-associated stroma (Fig. 1 *D* and *E*). These findings indicate that stromal cells in the thymic microenvironment become altered to support T-ALL survival and proliferation.

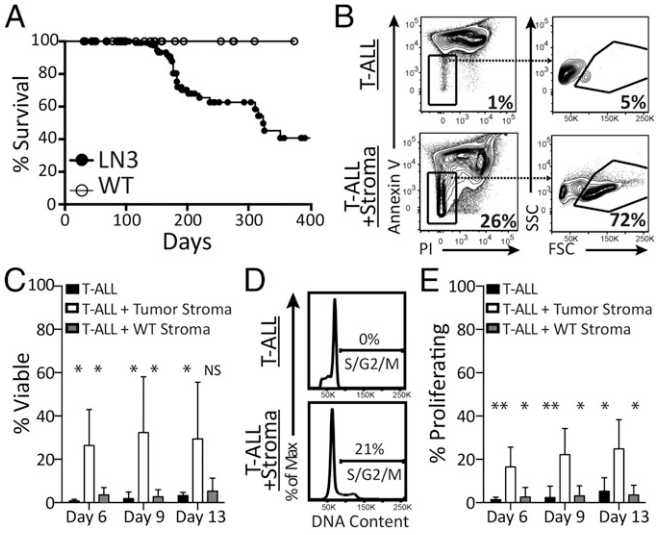

Fig. 1. LN3 thymic T-ALL cells require tumor stroma to survive and proliferate ex vivo. (*A*) Survival of indicated strains shown as Kaplan–Meier survival plots (n = 33, WT; n = 155, LN3). (*B–E*) Primary T-ALL cells were cultured with or without stromal cells enriched from mechanically dissociated LN3 thymic tumors or WT thymi. Representative flow cytometric plots evaluating viability (*B*) or DNA content (*D*) of viable cells 6 d after culture initiation. (*C* and *E*) The percentage of viable lymphoma cells (*C*) and viable cells in S/G_2/M (*E*) at the indicated number of days in culture. Graphs depict means + SD of cumulative data from duplicate wells from four independent experiments. $^*P < 0.05$ and $^{**}P < 0.01$.

The Thymic Epithelial Compartment Is Progressively Disrupted During T-ALL Tumorigenesis. Because tumor-associated, but not WT thymic, stromal cells supported lymphoma growth, we investigated compositional changes in the thymic microenvironments of LN3 mice during T-ALL progression. We first evaluated TECs because they provide signals essential for thymocyte development, including IL-7 and NOTCH ligands. In WT mice, the thymic epithelium consists of central Keratin-5^+ medullary TECs (mTECs) surrounded by Keratin-8^+ cortical TECs (cTECs). In LN3 mice, TEC organization was abnormal as early as 1 mo of age, with enlarged mTEC regions extending to the thymic capsule by 3 mo (Fig. 2*A*). In comparison with small isolated epithelial-free regions that can be found in the interior of some WT thymi (Fig. 2*A*) as previously described (23), strikingly large peripheral epithelial-free regions were abundant in LN3 thymic lymphomas, as seen in higher-magnification images (Fig. 2*A*) and in whole-thymic sections (Fig. 2*B*). These epithelial-free regions first appeared at the perimeter of pretumor LN3 thymi at 1 and 3 mo of age (Fig. 2 *A* and *B*). Thus, the thymic epithelium is progressively disorganized, culminating in expansion of extensive epithelial-free regions during LN3 T-ALL development.

Thymic Epithelial-Free Regions Are Enriched for Proliferating Lymphoma Cells Surrounded by Vasculature, Fibroblasts, and DCs. TECs are essential for thymocyte development and can support T-ALL survival in vitro (18), which led us to question whether tumor proliferation could be supported in epithelial-free regions. Surprisingly, $CD8^+$ tumor cells proliferate extensively in these regions, suggesting that nonepithelial cells in the tumor microenvironment likely support T-ALL growth (Fig. 3*A* and Fig. S1). To identify such alternate cell types, we quantified stromal cells from WT versus tumor-bearing LN3 thymi (phenotypes and gating strategies in Fig. S2). cTECs were largely absent in LN3 tumors, whereas mTECs were expanded. Strikingly, both the number and percentage of $Sirp\alpha^+$ DCs ($CD11c^{hi}EpCAM^-CD45^+MHCII^+Sirp\alpha^+CD80^+$ cells), one of two conventional thymic DC subsets (24), were greatly increased in tumor-bearing thymi (Fig. 3 *B* and *C*). Immunostaining revealed

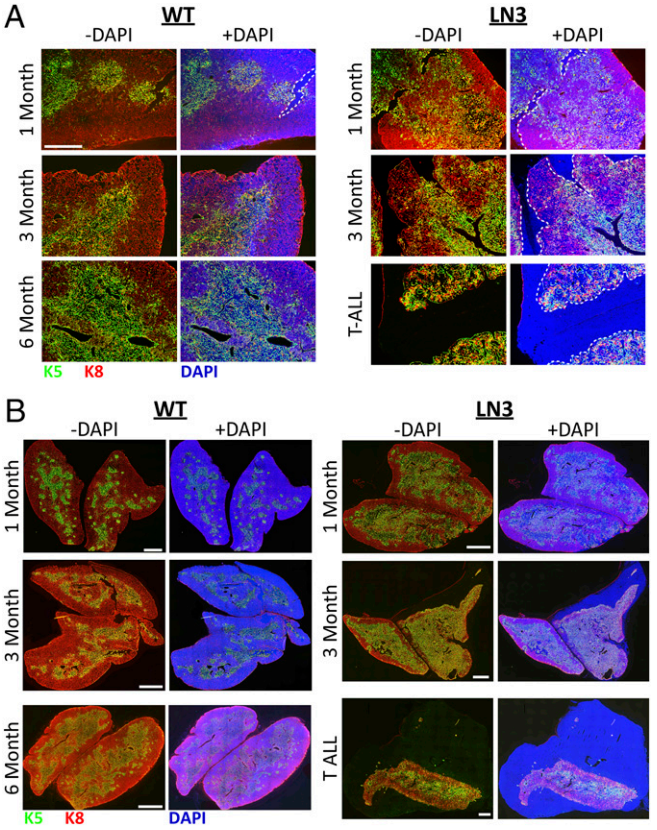

Fig. 2. Thymic epithelial-free regions emerge during T-ALL development. (*A*) Thymic cryosections from 1-, 3-, and 6-mo-old WT mice, from 1- and 3-mo-old tumor-free LN3 mice, and from a 6-mo-old tumor-bearing LN3 mouse, were immunostained for Keratin-5 (K5) and Keratin-8 (K8) with or without DAPI overlays. (Scale bar: 200 μm.) Borders of epithelial-free regions are denoted by white dotted lines. (*B*) Entire thymic cryosections from WT and LN3 mice immunostained as in *A* reveal overall changes in organization of the epithelium and emergence of peripheral epithelial-free regions as LN3 tumors form. (Scale bars: 1 mm.) Images in *A* and *B* are representative of three thymi at each stage and genotype.

that Sirpα$^+$ DCs were present in peripheral epithelial-free regions of LN3 thymic lymphomas; in contrast, DCs localize within central medullary regions of WT thymi (Fig. 3*D*). Epithelial-free regions in LN3 thymic tumors were also highly vascularized and contained extensive fibroblast/extracellular matrix (ECM) networks (Fig. 3*E*), consistent with a microenvironment supportive of tumor growth. Similar epithelial-free regions containing DCs, vasculature, and fibroblast networks were observed in thymic lymphomas from *LMO2* transgenic mice, which overexpress an oncogene frequently upregulated in human T-ALL (25) (Fig. 3 *D* and *E*). Primary patient T-ALL mediastinal mass sections also consisted of extensive epithelial-free regions containing dense DC networks, in contrast to the encompassing epithelial network and central DC localization in normal human thymi (Fig. 3*F*). All thymic lymphomas analyzed from the two mouse models and patient samples contained extensive epithelial-free regions with DC networks, suggesting commonality between tumor microenvironments in murine T-ALL of diverse oncogenic origins and in human T-ALL.

As in overt tumors, early epithelial-free thymic regions in young asymptomatic LN3 mice contained proliferating thymocytes (Fig. S3*A*), Sirpα$^+$ DCs (Fig. S3*B*), vasculature, and fibroblasts (Fig. S3*C*). In addition, the number and percentage of Sirpα$^+$ DCs increased with age in pretumor LN3 thymi but not in WT thymi (Fig. S3 *D*–*G*). Thus, microenvironments comparable to those in overt lymphomas emerge early and expand during T-ALL progression.

T-ALL Cells Require Contact with Tumor Stroma for Survival and Interact Extensively with DCs in the Thymic Microenvironment. Transwell assays revealed that T-ALL cells required close contact with tumor stroma to survive (Fig. 4*A*), similar to reports for chronic lymphocytic leukemia (26). Thus, we determined whether T-ALL cells made preferential contacts with stromal subsets in intact 3D thymic microenvironments. Using our previously established two-photon imaging approach (27), we compared the migration of WT thymocytes with LN3 tumor cells in live thymic slices containing EYFP$^+$ DCs (Fig. 4*B*) (28). Notably, LN3 T-ALL cells were in contact with thymic DCs twice as often as WT thymocytes (Fig. 4*C*) and exhibited a 190% increase in dwell time upon DC contact (Fig. 4*D*). Thus, LN3 tumor cells require contact with tumor stroma for survival ex vivo and interact extensively with thymic DCs in situ, which are positioned to provide mitogenic signals in epithelial-free regions within the tumor microenvironment.

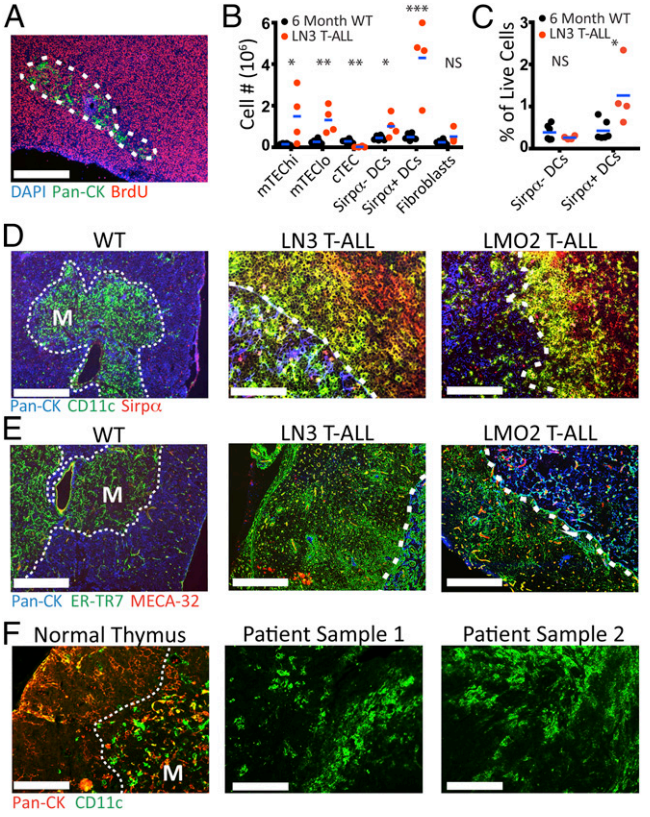

Fig. 3. Proliferating tumor cells are enriched in thymic epithelial-free regions containing DCs, fibroblasts, and vasculature. (*A*) Pan-Cytokeratin (Pan-CK) and BrdU immunostaining following a 20-min BrdU pulse reveals extensive proliferation of T-ALL cells in thymic epithelial-free regions. (Scale bar: 200 μm.) (*B* and *C*) Cellularity of thymic stromal subsets (*B*) and percentages of Sirpα$^-$ and Sirpα$^+$ DCs (*C*) in LN3 thymic lymphomas versus WT thymi from mice 6 mo of age. Graphs depict cumulative data from multiple experiments ($n = 6$, WT; $n = 4$, LN3 tumors); bars represent means. (*D* and *E*) WT and tumor-bearing LN3 and LMO2 thymic cryosections immunostained for Pan-Cytokeratin (Pan-CK), CD11c, and Sirpα (*D*) or Pan-CK, ER-TR7, and MECA-32 (*E*). (Scale bars: *D*, *Left* and *E*, 200 μm; *D*, *Center* and *Right*, 100 μm.) (*F*) Representative images of normal human thymic and T-ALL patient mediastinal mass sections immunostained for Pan-CK and CD11c. (Scale bars: *Left*, 100 μm; *Center* and *Right*, 50 μm.) Immunostains are representative of $n = 4$ (*A*), $n = 3$ (*D* and *E*), and $n = 4$ (*F*) biological replicates each. White dashed lines outline medullary regions (M) (thin lines) in WT/normal thymi and epithelial-free regions (thick lines) in thymic lymphomas. Few epithelial cells were identified in patient mediastinal mass sections. *$P <$ 0.05, **$P < 0.01$, and ***$P < 0.001$.

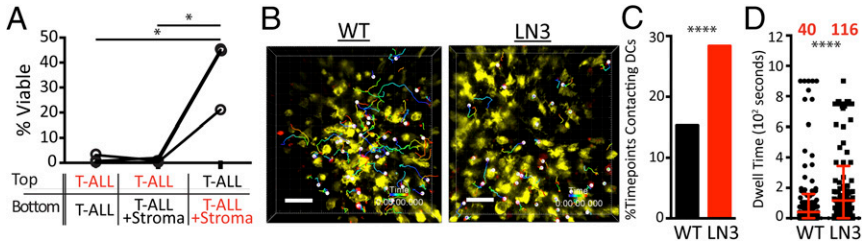

Fig. 4. LN3 lymphoma cells require close contact with stroma for ex vivo survival and make frequent and prolonged contacts with DCs in an intact thymic microenvironment. (*A*) Cocultures were initiated using transwell inserts to compartmentalize lymphoma cells and thymic tumor stromal cells, as indicated. Red axis labels indicate the chamber analyzed for viability after 6 d. Data from three experiments are shown, with each symbol representing the mean of duplicate wells. (*B–D*) Labeled WT thymocytes or LN3 lymphoma cells were imaged by two-photon microscopy in thymic slices from CD11c-EYFP mice. (*B*) Trajectories of WT and LN3 tumor thymocytes (red) migrating among thymic DCs (yellow) are displayed as color-coded tracks from start (blue) to end (red) of the time course. White spheres indicate tracked cells. See corresponding movies (Movies S1 and S2). Cell tracking was used to calculate the percentage of time points in which cells contacted DCs (*C*) and the duration of DC contacts (*D*). Graphs represent cumulative data from five experiments. (*C*) Data were calculated from cumulative time points (n = 15,706: WT; n = 13,048: LN3) of all tracked cells. (*D*) Means ± SD from cumulative tracked cells (n = 505, WT; n = 306, LN3) are displayed in red on the plots. Dots represent individual cells; mean values are displayed above the graph. *P < 0.05 and ****P < 0.0001.

Myeloid Cells from Primary Tumor Microenvironments Promote Lymphoma Survival ex Vivo. To identify the endogenous tumor stromal cell types capable of supporting survival of LN3 T-ALL cells, we cocultured primary tumor cells with sorted stromal subsets from the same tumors. Cocultures containing a combination of all sorted stromal subsets ("All Stroma") resulted in an average of 52% lymphoma viability after 6 d (range of viability, 24–78%; stromal phenotypes and sort purities in Fig. S4 *A–C*). To control for variable survival between experiments with different primary tumors, we normalized T-ALL viability to cultures containing All Stroma for each experiment. Depletion of epithelial cells or fibroblasts had no effect on tumor survival ex vivo (Fig. 5*A*). Strikingly, depletion of myeloid cells or DCs alone resulted in a significant decrease in the viability of T-ALL cells (Fig. 5*A*). Conversely, sorted tumor-associated DCs and/or $CD11c^{-}CD11b^{+}$ myeloid cells were sufficient to support T-ALL survival (Fig. 5*A*). However, when an equal number of DCs or $CD11c^{-}CD11b^{+}$ myeloid cells were cocultured with T-ALL cells, DCs promoted growth of 6.5-fold more viable T-ALL cells on average (Fig. 5*B*). CD3 and CD8 expression confirmed that the majority of viable cells were T-ALL cells and not stromal subsets in all coculture conditions (Fig. S4*D*). Collectively, these results demonstrate that myeloid cells, and particularly DCs from the thymic tumor microenvironment, are necessary and sufficient to support T-ALL survival and growth.

Thymic DCs Are Functionally Altered in T-ALL. The unique ability of tumor-derived stroma to support T-ALL growth ex vivo (Fig. 1 *C–E*) could reflect functional changes in DCs or an increase in DC cellularity during tumor progression. Thus, we compared the ability of an equivalent number of WT versus tumor-associated thymic DCs to support T-ALL survival. Only tumor-associated DCs supported significant T-ALL viability, demonstrating that DCs in the tumor microenvironment have enhanced tumor-promoting capabilities (Fig. 5*C*; DC purity shown in Fig. S5*A*). Distinguishing DCs from macrophages based on CD11c expression is not always dependable, especially in tumor microenvironments (29). LN3 tumor-associated DCs are phenotypically consistent with assignment to the DC lineage in that they express high levels of CD11c, MHC-II, and CD80 (Fig. S2). To further confirm the DC identity of tumor-supportive cells, we transcriptionally profiled DCs from LN3 thymic lymphomas and WT thymi, revealing that tumor-associated DCs express the DC-specific transcription factor *Zbtb46* (30) (https://gexc.stanford.edu/models/1118/genes). Furthermore, hierarchical clustering of transcriptional profiling data from tumor-associated DCs, WT thymic DCs, and other WT myeloid subsets revealed that tumor-associated DCs were most closely related to their WT thymic DC counterparts and were distinct from macrophages and monocytes (Fig. 5*D*) (31).

DCs from Metastatic Tumors Support T-ALL Growth ex Vivo. As in the primary thymic tumor, T-ALL cells from metastatic lymph nodes and spleens died when cultured alone but survived in the presence of tumor-associated stroma from their respective organs (Fig. 6*A*). Flow cytometric analyses revealed a significant increase in the number of DCs ($CD11c^{+}B220^{-}$) and a consistent, although nonstatistically significant, increase in the number of $CD11c^{-}CD11b^{+}$ myeloid cells in tumor-bearing lymph nodes and spleens, resulting in maintenance of the DCs' proportional representation in these metastatic organs (Fig. 6*B* and Fig. S5 *B* and *C*). Importantly, tumor-associated splenic DCs were necessary and sufficient to promote survival of splenic T-ALL cells (Fig. 6*C*) and could also support survival of T-ALL cells from primary thymic lymphomas and metastatic lymph nodes (Fig. 6*D*). Conversely, splenic versus thymic DCs from the same tumor-bearing mice had a comparable capacity to support survival of splenic T-ALL cells (Fig. 6*E*). Together, these data demonstrate that tumor cells from primary and metastatic tumor sites require DC-mediated support for survival and that DCs at both primary and metastatic sites are comparably poised to promote survival of circulating T-ALL cells.

PDGFRβ and IGF1R Are Up-Regulated on T-ALL Cells with Concomitant Expression of Cognate Ligands by Tumor-Associated DCs. To identify potential pathways governing DC-mediated lymphoma survival, we analyzed gene expression profiles of sorted murine T-ALL cells for overexpression of growth factor receptors whose ligands were expressed by tumor-associated DCs. *Pdgfrb* and *Igf1r* were highly expressed by T-ALL cells (Fig. 7*A*), whereas the ligands *Pdgfa*, *Pdgfb*, *Pdgfc*, and *Igf1* were expressed by tumor-associated DCs (Fig. 7*B*). Expression of these ligands was specific, because *Pdgfd* and *Igf2* were not expressed. Tumor-associated $Sirp\alpha^{+}$ DCs expressed higher levels of *Pdgfc* and *Igf1* than $Sirp\alpha^{-}$ DCs. Expression data from tumor-associated and WT thymic DC subsets, T-ALL cells, and WT thymocyte subsets are provided in a searchable model within Gene Expression Commons (https://gexc.stanford.edu/models/1118/genes) (32).

Immunostaining and flow cytometry confirmed high expression of PDGFRβ protein on T-ALL cells in thymic and metastatic tumors from LN3 and LMO2 mice (Fig. 7*C* and Fig. S6 *A* and *B*), while PDGFRβ is expressed mainly on pericytes in WT thymi. Interestingly, PDGFRβ expression is apparent on sparse thymocytes in some pretumor tissues (Fig. 7*D* and Fig. S6*C*), suggesting PDGFRβ up-regulation is a characteristic of T-ALL development rather than a general peculiarity of thymocytes in LN3 and LMO2 murine T-ALL models.

We also evaluated PDGFRβ expression in T-ALL patient thymic and metastatic lymph node samples. One of eight patient lymph nodes evaluated displayed elevated PDGFRβ expression on tumor cells (Fig. 7*E*), indicating that PDGFRβ overexpression occurs in a subset of T-ALL patients. Analysis of previously reported expression profiling data from primary patient samples revealed higher expression of *PDGFRB* in the early T-cell precursor (ETP) T-ALL subset (Fig. 7*F*) (25, 33), suggesting elevated PDGFRβ expression is

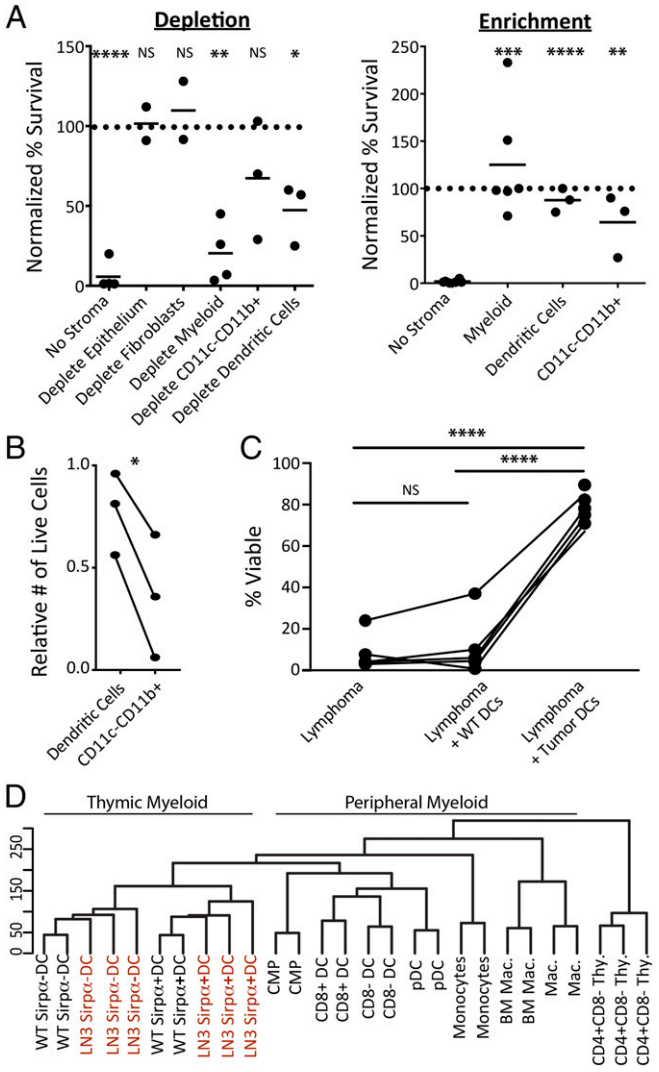

Fig. 5. Tumor-associated thymic myeloid cells are necessary and sufficient to support T-ALL survival. (*A*) LN3 T-ALL cells were cultured with or without sorted stromal subsets from thymic tumors; viability was assessed after 6 d. Results are normalized to the percentage of live cells in cocultures containing All Stroma for each experiment. Graphs depict cumulative data from multiple experiments, with each dot representing the mean of duplicate wells; bars represent means of all experiments. For statistical analysis, the depleted subsets (*Left*) were compared with All Stroma and enriched subsets (*Right*) were compared with "No Stroma." (*B*) The number of live cells from cocultures with the indicated sorted myeloid subsets in *A* relative to All Stroma cocultures. (*C*) LN3 T-ALL cells were cocultured with or without an equivalent number of DCs enriched from LN3 thymic tumors or WT thymi; viability was assessed at day 6. Graphs depict cumulative data, with each line representing survival from individual experiments (*B* and *C*). (*D*) Hierarchical clustering of the indicated cell subsets was performed using global gene expression data. Red text indicates tumor-associated DC subsets. $*P < 0.05$, $**P < 0.01$, $***P < 0.001$, and $****P < 0.0001$.

associated with a more aggressive form of T-ALL (34). Medyouf et al. previously reported that IGF1R is a transcriptional target of NOTCH1 that is expressed on human T-ALL cells (35). Together, these findings reveal that elevated expression of PDGFRβ and IGF1R are shared characteristics of mouse and human T-ALL.

Tumor-Associated DCs Activate IGF1R in T-ALL Cells. To determine whether the T-ALL tumor microenvironment supplies endogenous signals that activate PDGFRβ and IGF1R, we analyzed the phosphorylation status of these receptors in tumor cells directly ex vivo. Phosphorylation of PDGFRβ (pPDGFRβ) and IGF1R (pIGF1R) was elevated in T-ALL cells relative to WT thymocytes (Fig. 8*A*). We next evaluated whether tumor-associated and/or WT DCs could activate PDGFRβ and IGF1R in T-ALL cells. Tumor-associated DCs sustained activation of IGF1R in lymphoma cells throughout 7 d of culture, whereas WT DCs did not (Fig. 8 *B* and *C*). After only 24 h of culture, a time point that precedes apoptosis of T-ALL cells cultured alone, the majority of T-ALL cells cocultured with tumor-associated DCs had activated IGF1R (Fig. 8*B*), indicating that tumor-associated DCs signal to the majority of T-ALL cells, rather than to a rare tumor-initiating subset. The specificity of pIGF1R and pPDGFRβ staining on T-ALL cells was verified using fluorescence minus one (FMO) and isotype controls, along with specific IGF1R inhibitors (Fig. S7 *A*–*C*). The ability of tumor-associated, but not WT, DCs to sustain IGF1R activation is consistent with higher gene expression of *Igf1* by tumor-associated Sirpα$^+$ DCs relative to WT DCs (Fig. 8*D*). Furthermore, tumor-associated DCs secrete elevated levels of IGF1 protein relative to WT DCs (Fig. 8*E*). These findings suggest that up-regulation of IGF1 by tumor-associated DCs could enable them to support T-ALL survival. In contrast, PDGFRβ was not activated by tumor-associated DCs (Fig. 8*B*), despite high expression of the *Pdgfc* transcript by tumor-associated DCs and activation of PDGFRβ in ex vivo T-ALL cells (Figs. 7*A* and 8*A*). Because PDGF-C is latent and thought to inhibit PDGFR signaling until proteolytically activated in the extracellular compartment (36), PDGF-C made by DCs in culture may not be activated to promote PDGFRβ signaling in T-ALL cells.

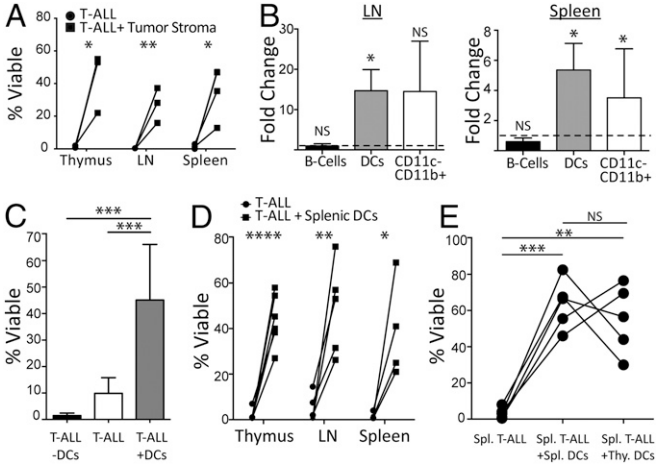

Fig. 6. T-ALL cells at metastatic sites require stromal support, and expanded DCs from metastatic lymphoid organs are sufficient to support T-ALL survival. (*A*) T-ALL cells from thymi, lymph nodes, or spleens were cultured with or without tumor-associated stroma from the same organ, as in Fig. 1; viability was assessed at day 6. Each line represents data from an individual experiment. (*B*) Mean fold change in cellularity of the indicated cell types in lymph nodes and spleens of tumor-bearing LN3 mice relative to WT mice. Graphs depict the means + SD of cumulative data ($n = 5$, LN3; $n = 2$, WT). The dotted line indicates a fold change of 1. (*C*) Single-cell suspensions of splenic T-ALL cells were cultured alone, following depletion of DCs, or in the presence of additional tumor-associated splenic DCs; T-ALL viability was assessed after 6 d. Bars represent means + SD from five experiments. (*D*) T-ALL cells from thymi, lymph nodes, or spleens, as indicated, were cultured with or without splenic DCs from the same tumor-bearing mice. (*E*) Splenic T-ALL cells were cultured after myeloid depletion or with addition of DCs from the spleen or thymus from the same tumor-bearing mouse. (*D* and *E*) Lines connect the average of duplicate wells for each condition from individual experiments. $*P < 0.05$, $**P < 0.01$, $***P < 0.001$, and $****P < 0.0001$.

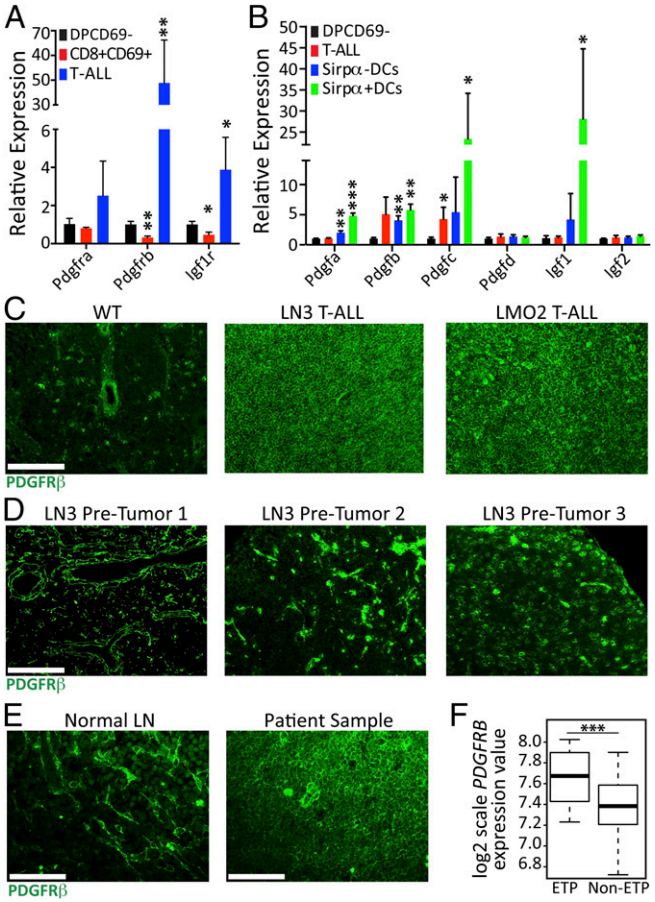

Fig. 7. Elevated expression of IGF1R and PDGFRβ on T-ALL cells and expression of ligands by tumor-associated DCs. (*A* and *B*) Relative gene expression of the indicated growth factor receptors in T-ALL cells and WT thymocyte subsets (*A*) and associated growth factors in tumor-associated DC subsets, T-ALL cells, and WT thymocytes (*B*). (*A* and *B*) Expression is normalized to WT DP69- thymocytes. Graphs depict the means + SD of data from three experiments. (*C*) Representative images ($n = 3$ each) of a WT thymus and an LMO2 and LN3 thymic lymphoma immunostained for PDGFRβ. (Scale bars: 100 μm.) (*D*) Representative images of cryosections from three pretumor LN3 thymi immunostained for PDGFRβ. (Scale bars: 100 μm.) (*E*) Representative images of a nonmalignant and metastatic T-ALL human lymph node (LN) immunostained for PDGFRβ. (Scale bars: 50 μm.) Overexpression of PDGFRβ was seen on one LN of eight patient sections (four LN and four mediastinal mass). (*F*) Log_2 gene expression values for *PDGFRB* in ETP ($n = 12$) and non-ETP ($n = 66$) T-ALL cases. *P* values were generated by pairwise *t* tests in Limma ($P = 0.0002$; false-discover rate, 0.012). $^*P < 0.05$, $^{**}P < 0.01$, and $^{***}P < 0.001$.

Activation of the MAPK Pathway Is Associated with IGF1R Signaling in T-ALL Cells. Activation of the MAPK pathway has been implicated in pathogenesis of several cancers (37). Compared with WT thymocytes, ex vivo thymic lymphoma cells had elevated MAPK signaling, as indicated by increased levels of phosphorylated Erk (pErk) (Fig. S8*A*). Coculture with tumor-associated, but not WT, thymic DCs sustained pErk over 7 d (Fig. S8*A*). IGF1R signaling can activate the MAPK cascade, supporting survival of mature T cells and other tumors (38, 39). Therefore, we evaluated coexpression of pIGFR1 with pErk. Levels of pIGF1R consistently correlated with pERK levels both in ex vivo T-ALL cells and following coculture with tumor-associated DCs (Fig. S8 *B–D*). Specificity of pERK staining was verified with FMO and isotype controls (Fig. S7 *A* and *B*). Furthermore, inhibiting IGF1R signaling resulted in decreased pErk levels (Fig. S8*E*). IGF1R activation also correlated with T-ALL cellular proliferation ($Ki67^+$) (Fig. S8*F*). Together, these data indicate that IGF1R signaling activates the MAPK pathway and promotes proliferation of T-ALL cells.

DC-Mediated T-ALL Survival Is Dependent on IGF1R Signaling. IGF1 has been shown to directly support growth of solid and hematological malignancies (35, 39–41). To determine whether IGF1R signaling was required for DC-mediated T-ALL survival, we treated thymic and splenic T-ALL:DC cocultures with graded concentrations of three structurally distinct IGF1R inhibitors: AG-1024 (42), picropodophyllin (PPP) (43), and BMS-754807 (44). All three inhibitors decreased survival of primary and metastatic T-ALL cells in a dose-dependent manner (Fig. 9*A*), with IC_{50} values in the range reported for other tumor studies (40, 41, 44–46). AG-1024 and PPP were chosen because they are reported to have few off-target effects (45, 46); we validated that AG-1024 and PPP inhibited IGF1R activation (Fig. S7*C*). Notably siRNA-mediated knock down of *Igf1r* also resulted in a reduction in T-ALL cells expressing pIGF1R (Fig. 9*B*), with a concomitant decrease in T-ALL survival (Fig. 9*C*) and proliferation (Fig. 9*D*). These findings demonstrate that DC-mediated T-ALL survival in the LN3 model is IGF1R-dependent.

To determine whether DC-mediated survival and activation of IGF1R, ERK, and PDGFRβ are common features of independent models of T-ALL, we evaluated LMO2 transgenic tumors. As in the

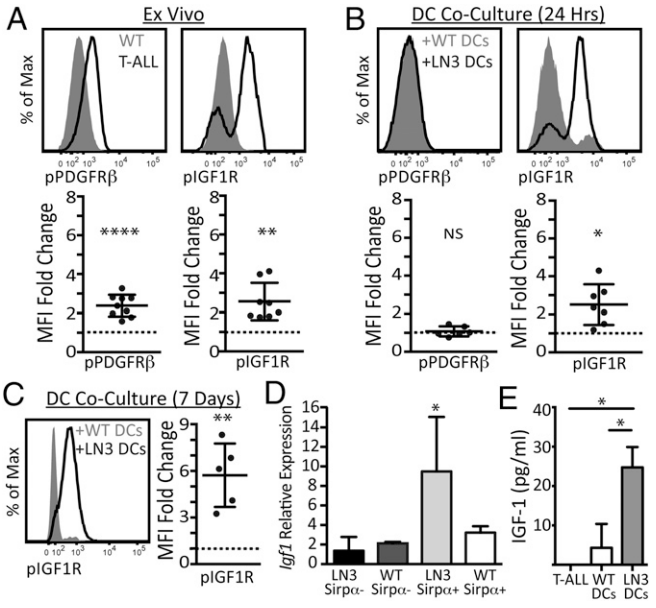

Fig. 8. Tumor-associated DCs sustain IGF1R activation but not PDGFRβ. (*A*) Representative flow cytometric plots of pPDGFRβ and pIGF1R in viable cells from WT and tumor-bearing LN3 thymi examined ex vivo. Graphs depict the mean fluorescence intensity (MFI) fold change of pPDGFRβ and pIGF1R in viable T-ALL cells versus WT thymocytes; each dot represents an individual tumor/WT control analyzed in the same experiment; bars represent the means ± SD. The dotted line indicates a fold change of 1. (*B* and *C*) Representative flow cytometric plots of pPDGFRβ and pIGF1R levels in viable thymic LN3 T-ALL cells after 24 h (*B*) or 7 d (*C*) in culture with DCs enriched from WT or tumor-bearing LN3 thymi. Graphs depict the MFI fold change of pPDGFRβ and pIGF1R in T-ALL cells cultured with tumor-associated versus WT DCs; dots represent individual tumors; bars represent means ± SD. (*D*) Relative *Igf1* expression levels in DC subsets from WT and tumor-bearing LN3 thymi normalized to LN3 $Sirp\alpha^-$ DCs. Means + SD from two WT DC and three LN3 DC datasets are shown. (*E*) Quantification of IGF1 concentrations in the supernatants of wells containing 1×10^5 DCs enriched from WT ($n = 2$) or LN3 tumor-bearing thymi ($n = 3$) or from thymic T-ALL cells depleted of $CD11c^+$ and $CD11b^+$ myeloid cells ($n = 3$). Cultures were established for 24 h, and duplicate wells were averaged for each experiment. $^*P < 0.05$, $^{**}P < 0.01$, and $^{****}P < 0.001$.

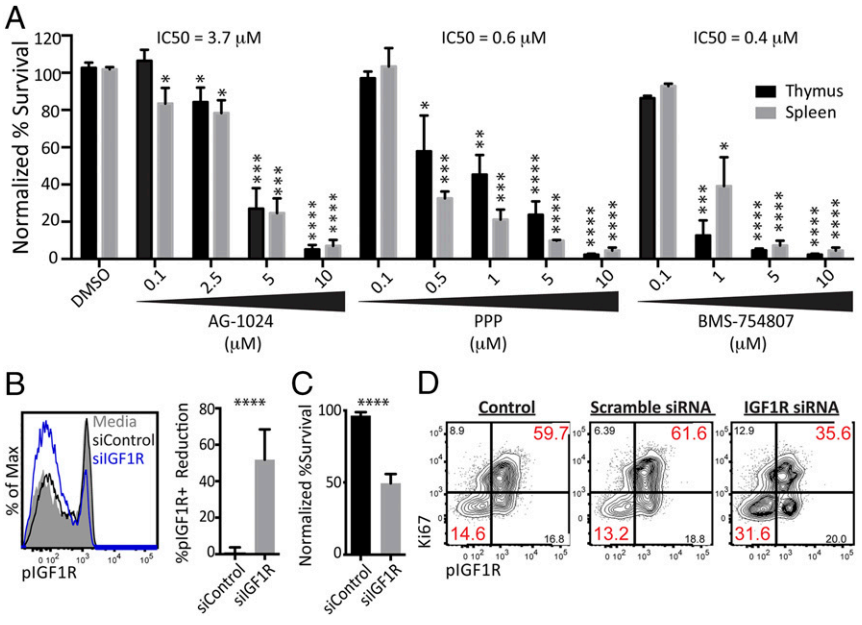

Fig. 9. IGF1R signaling is required for DC-mediated T-ALL survival. (*A*) Primary LN3 splenic or thymic T-ALL cells were cultured for 4 d with tumor-associated DCs from the same organ before addition of the IGF1R small-molecule inhibitors AG-1024, PPP, or BMS-754807, as indicated. Viability was assessed after 3 d. Bars represent the means + SD from three to seven experiments for each condition normalized to cocultures containing a DMSO vehicle control. The IC_{50} values are indicated above the graphs. (*B–D*) T-ALL cells were cultured with tumor-associated DCs in the presence or absence of IGF1R-targeted siRNA (2.5 μM) or a nontargeted siRNA control (2.5 μM); 6 d after culture initiation, T-ALL cells were evaluated by flow cytometry for pIGF1R levels (*B*), viability (*C*), and IGF1R activation versus proliferation by Ki67 (*D*). Flow cytometric plots are representative of four independent experiments. The graph in *B* depicts the percentage reduction of $pIGF1R^+$ T-ALL cells in the indicated siRNA treatment groups compared with control wells without siRNA. The graph in *C* depicts T-ALL viability normalized to control wells without siRNA. Graphs in *B* and *C* represent cumulative data + SD from four tumors analyzed in independent experiments. $*P < 0.05$, $**P < 0.01$, $***P < 0.001$, and $****P < 0.0001$.

LN3 model, LMO2 T-ALL cells survived only if cocultured with tumor-associated DCs (Fig. S9*A*). When examined directly ex vivo, LMO2 T-ALL cells had elevated levels of pIGF1R, pErk, and pPDGFRβ relative to WT thymocytes (Fig. S9*B*). Furthermore, IGF1R phosphorylation correlated with Erk phosphorylation in T-ALL cells analyzed ex vivo and correlated with ERK activation and proliferation in T-ALL cells cocultured with tumor-associated DCs (Fig. S9 *C* and *D*). Importantly, as in the LN3 model, inhibition of IGF1R signaling abrogated DC-mediated survival of LMO2 T-ALL cells (Fig. S9*E*). Altogether, these studies provide the first indication to our knowledge that DCs in the tumor microenvironment directly support survival and growth of T-ALL cells in an IGF1R-dependent manner.

Discussion

In this study, we demonstrate that the thymic microenvironment becomes altered during LN3 T-ALL progression such that DCs gain the capacity to support T-ALL growth. Human primary T-ALL samples require stromal-derived signals for survival (10, 16), suggesting such signals, if identified, could be viable therapeutic targets. Previous studies revealed that in the presence of exogenous cytokines, TECs from healthy thymi and bone marrow (BM) cell lines could support T-ALL (10, 16–18). However, endogenous tumor stromal cells capable of supporting T-ALL growth in the absence of exogenous cytokines have not been previously identified.

We initially focused on TECs because they express IL-7 and NOTCH ligands, which have been implicated in supporting T-ALL. However, we found that epithelial-free regions enriched for proliferating lymphoma cells emerged at the periphery of thymic tumors in two distinct T-ALL models, consistent with epithelial-free regions in thymic tumors that arise in AKR mice (23). Epithelial-free regions also comprised the majority of tissue in mediastinal mass sections from T-ALL patients. These findings, along with the fact that TECs are confined to thymi and, thus, are not present to support T-ALL growth at metastatic sites, indicated that other stromal subsets must support T-ALL.

Unexpectedly, we found that tumor-associated myeloid cells, particularly DCs, were necessary and sufficient to support survival and growth of T-ALL cells in vitro. Given that thymic DCs generally induce negative selection of autoreactive thymocytes, it was surprising that these DCs would provide survival signals to tumors derived from developing T cells. In contrast, DCs in secondary lymphoid organs prototypically promote T-cell proliferation and survival during T-cell activation and in homeostasis. In keeping with this function in the periphery, a previous study demonstrated that DCs could directly support survival of cutaneous T-cell lymphoma cells in vitro (47). Additionally, T-ALL–promoting activity was not exclusive to DCs located in primary thymic tumors, because DCs from tumor-bearing spleens and thymi promoted T-ALL survival equivalently. Furthermore, tumor cells at both primary and metastatic sites required the presence of DCs for survival. Thus, T-ALL cells first interact with altered DCs in the thymic tumor environment that can promote their survival, and as T-ALL cells seed metastatic sites, they encounter peripheral DCs poised to sustain their growth. DCs were also present throughout patient mediastinal mass sections and lymph nodes, indicating that DCs are positioned to support human T-ALL growth as well. Collectively, these results suggest that targeted therapies against DCs or their tumor-promoting signals would affect tumor growth at both primary and metastatic tumor sites.

We found that IGF1R signaling was required for DC-mediated murine T-ALL growth in two molecularly distinct murine models of T-ALL. Exon sequencing revealed that many LN3 tumors have activating *Notch1* mutations, and some LMO2 tumors are also NOTCH-driven (25). Thus, DCs and IGF1R signaling can promote survival of NOTCH-driven murine T-ALL cells. All of the LN3 and LMO2 tumors analyzed required DC-mediated support for survival in vitro, but some of the LN3 tumors did not have detectable activating mutations in *Notch1*, suggesting that DCs may also support growth of other molecular subsets of T-ALL. IGF1R activation is likely relevant to human T-ALL growth as well. Activating mutations in *NOTCH1* have been reported in >50% of T-ALL cases (22), and activated NOTCH1 induces IGF1R expression in mouse and human T-ALL cells (35, 48). Importantly, IGF1R expression contributes to T-ALL leukemia-initiating cell activity in vivo, and inhibition of IGF1R signaling prolongs survival following transplantation of T-ALL in mice (35). Previous studies in other cancers have demonstrated that IGF1R signaling confers resistance to traditional therapies (49), providing a rationale for combining IGF1R-targeted therapy with standard treatments (e.g., chemotherapy and radiation) or in conjunction with inhibitors of other pathways.

Although we found that IGF1R signaling was necessary for DC-mediated T-ALL survival, other myeloid-derived factors likely contribute to T-ALL progression in vivo. Transwell assays

revealed that T-ALL cells required close contact with tumor stroma to survive. Because IGF1 is secreted, other transmembrane molecules may therefore mediate interactions between tumor cells and DCs. Tumor–DC interactions could promote localized delivery of IGF1 to T-ALL cells and/or could induce signaling through alternate mitogenic pathways. In addition, gene ontology (GO) analysis comparing tumor-associated versus WT thymic DCs revealed that tumor-associated DCs have increased expression of genes involved in "response to wound healing" ($P = 21.4 \times 10^{-11}$) and "inflammatory responses" ($P = 1.3 \times 10^{-8}$). Some of these genes, which are associated with alternatively activated (M2) macrophages and TAMs (*Chi3l3*, *Retnla*, and *Arg1*), have been implicated in growth of several tumors (4, 50, 51). Like *Igf1*, these genes were up-regulated to a greater degree in the Sirpα$^+$ subset of thymic DCs, which are numerically expanded in thymic lymphomas (https://gexc.stanford.edu/models/1118/genes). These findings suggest that Sirpα$^+$ DCs are most capable of supporting T-ALL growth, although our data demonstrate that other myeloid cells likely contribute. Similarly, monocytes differentiated into M2 macrophages were shown to directly promote proliferation of adult T-cell leukemia/lymphoma cell lines (52). Thus, it will be important to evaluate the respective roles of tumor-associated Sirpα$^+$ and Sirpα$^-$ DCs, as well as other myeloid subsets in supporting T-ALL growth.

It is not clear why *Pdgf* genes expressed by tumor-associated DCs did not sustain activation of PDGFRβ in T-ALL cells in vitro. Although *Pdgfa* and *Pdgfb* may not be expressed at sufficiently high levels, *Pdgfc* was expressed robustly by tumor-associated Sirpα$^+$ DCs; however, PDGF-C stimulates PDGFRαα and αβ heterodimers, instead of the PDGFRββ receptor found to be up-regulated on LN3 T-ALL cells (36). Furthermore, PDGF-C and -D block binding to PDGFRββ before their activation by extracellular proteolytic cleavage, which may not occur in in vitro DC cocultures (36). Although tumor-associated DCs were not sufficient to sustain activation of PDGFRβ in cocultures, the receptor was phosphorylated in T-ALL cells analyzed ex vivo, indicating the tumor microenvironment activates PDGFRβ. Extensive vascularization and fibroblast/ECM networks were present in the aberrant T-ALL tumor microenvironment, and fibroblasts and endothelial cells may provide high levels of PDGFs and activating proteases in vivo (36). Thus, PDGFRβ signaling may be sustained by DCs and/or other tumor stromal subsets in the tumor microenvironment, which may contribute to T-ALL progression.

We hypothesize that PDGFRβ is also relevant to human T-ALL, because *PDGFRB* expression was elevated in a subset of T-ALL patient samples, and PDGFRβ was overexpressed on T-ALL cells in a primary patient lymph node. Furthermore, PDGF receptors are up-regulated in mature T-cell lymphomas (53–56), and a translocation involving *PDGFRB* has been identified in a T-ALL patient (53). To our knowledge, we provide the first evidence that PDGFRβ is up-regulated preferentially in ETP T-ALLs. Gene expression profiling of WT thymocytes demonstrates that PDGRβ is normally expressed on ETPs and subsequently down-regulated as the cells differentiate (https://gexc.stanford.edu/models/1118/genes). Thus, inappropriate maintenance of this growth factor receptor may contribute to tumorigenesis of the immature and aggressive ETP T-ALL subset. Importantly, remission of a patient with refractory anaplastic large cell lymphoma was recently achieved with a PDGFRβ inhibitor, imatinib (55), highlighting the potential of targeting PDGFRβ in other T-cell malignancies. However, our studies demonstrate that DCs promote T-ALL survival through IGF1R activation in the absence of PDGFRβ signaling. Thus, whereas targeting PDGFRβ may be warranted in a subset of T-ALL patients with up-regulated receptors, PDGFRβ inhibition may be efficacious only in combination with other standard regimens or targeted agents, such as IGF1R inhibitors.

In summary, we identify DCs as an endogenous cell type in the tumor microenvironment that becomes altered during T-ALL progression to gain the capacity to directly support tumor growth through IGF1R signaling. To our knowledge, this is the first demonstration that (*i*) DCs from the tumor microenvironment directly support T-ALL survival, (*ii*) DCs are a source of IGF1 mitogenic signals that promote T-ALL survival, and (*iii*) PDGFRβ is up-regulated on an aggressive subset of human T-ALLs and is activated by the tumor microenvironment in two distinct murine T-ALL models. Notably, DCs can prime antitumor adaptive immune responses; thus, different DC subsets likely have the opposing roles of either promoting T-ALL growth, as shown here, or controlling T-ALL growth via activation of antitumor immune responses. It will be important to determine which specific DC subsets directly support T-ALL growth, so as to assess the therapeutic potential of targeting these subsets and their tumor promoting signals in vivo, while leaving intact the capacity to mount antitumor immune responses. Thus, our findings provide a strong rationale for further investigation of DC-mediated T-ALL growth to identify novel therapeutic targets.

Materials and Methods

Mice. LN3 mice were provided by Tom Serwold, Joslin Diabetes Center, Boston (21). C57BL/6J and CD11c-EYFP [B6.Cg-Tg(Itgax-EYFP)1Mnz/J] mice were purchased from The Jackson Laboratory. LN3 and LMO2 (B6.CD2-Lmo2) (25) mice were euthanized upon lymphoma detection, as identified by enlarged lymph nodes, hunched posture, reduced motility, ruffled fur, and/or labored breathing. All mice were housed under specific pathogen-free conditions at The University of Texas at Austin (UT Austin) and the Eunice Kennedy Shriver National Institute of Child Health and Human Development, National Institutes of Health (NICHD/NIH). Experimental procedures were approved by the Institutional Animal Care and Use Committee at UT Austin or the Animal Care and Use Committee at the NICHD/NIH.

Notch1 Exon Sequencing. DNA was extracted from 5×10^6 WT thymocytes or primary LN3 T-ALL cells using the DNeasy Blood and Tissue Kit (Qiagen). *Notch1* exons 26 and 27 were amplified with the following primer sets: 26 forward, 5′-ACGGGAGGACCTAACCAAAC-3′; 26 reverse, 5′-CAGCTTGGTCTCCAACACCT-3′; 27 forward, 5′-CGCTGAGTGCTAAACACTGG-3′; and 27 reverse, 5′-GTTTTGCCTGCATGTACGTC-3′. Exon 34 was amplified in two fragments using the following primer sets: 34.1 forward, 5′-GCTCCCTCATGTACCTCCTG-3′; 34.1 reverse, 5′-TAGTGGCCCCATCATGCTAT-3′; 34.2 forward, 5′-ATAGCATGATGGGGCCACTA-3′; and 34.2 reverse, 5′-CTTCACCCTGACCAGGAAAA-3′. These primer sets have been previously described (57). PCR products were purified using a PCR purification kit (Qiagen) and sequenced directly at the UT Austin Institute for Cellular and Molecular Biology Genome Sequencing and Analysis Facility. *Notch1* sequences from T-ALL were compared against those from WT thymocytes using the novoSNP analysis program (58). A cutoff score of 1 and *F* score of 1 were used to identify mutations that were then verified only if forward and reverse primers revealed the same mutation. The ApE program (A plasmid Editor version 2.0.49 by M. Wayne Davis, University of Utah, Salt Lake City) was used for translating exon-sequencing results into protein sequences.

Patient Samples. Lymph node and mediastinal mass tissue samples from T-ALL patients were collected and provided by the Texas Children's Hospital, and deidentified, formalin-fixed, paraffin-embedded tissue sections were provided for analysis with approval from the institutional review board committees at UT Austin and Texas Children's Hospital.

Immunostaining and Microscopy. Immunostaining of murine tissue was performed on 7-μm acetone-fixed cryosections according to standard protocols. The following antibodies were used: anti-CD11c (N418), anti–Pan-Endothelial Cell Antigen (MECA-32), anti-fibroblast/ECM (ER-TR7), anti-Keratin5 (polyclonal; Covance), anti-Sirpα (p84), anti–Pan-Cytokeratin (C-11), anti-Keratin8 (TROMA-1), anti-CD3 (17A2), and anti-PDGFRβ (APB5). To detect proliferation, mice were injected intraperitoneally with 2 mg of 5-bromo-2′-deoxyuridine (BrdU) 20 min before euthanasia, and thymic cryosections were stained with anti-BrdU and anti-CD8 (53-6.7) per standard protocols.

Immunostaining of formalin-fixed, paraffin-embedded patient tissue samples followed standard protocols. Slides were incubated with: anti–Pan-Cytokeratin (AE1/AE3), anti-CD11c (EP1347Y), and anti-PDGFRβ (28E1). Primary antibodies

were detected with fluorochrome-conjugated anti-Ig (Jackson ImmunoResearch), or streptavidin (Life Technologies).

Images were acquired using an Axio Imager A1 microscope (Zeiss), with an AxioCam MRm camera (Zeiss); Zeiss EC Plan-Neofluar 5×/0.16, Plan-Apochromat 10×/0.45, and Plan-Apochromat 20×/0.8 objectives; and AxioVision 4.8 software (Zeiss). Adobe Photoshop version 12.0 was used for overlays of fluorescent channels and to adjust exposure uniformly across the images. Composite immunofluorescence images were acquired with an Eclipse 80i microscope (Nikon), a CoolSNAP HQ^2 camera (Photometrics), and a 10×/0.3 CFI Plan Fluor objective (Nikon) and were stitched using NIS Elements 3.0 (Nikon).

Flow Cytometry. For thymic stromal subsets, WT and tumor-bearing thymi were enzymatically digested with a combination of Collagenase IV and Dispase as described (59). Single-cell suspensions were immunostained with *Ulex europaeus* agglutinin I (UEA-1), anti-CD3 (145-2C11), anti-CD8 (53-6.7), anti-CD11c (N418), anti-I-A/I-E (M5/114.15.2), anti-CD45 (30-F11), anti-CD11b (M1/70), anti-B220 (RA3-6B2), anti-TER-119 (TER-119), anti-CD31 (390), anti-EpCAM (G8.8), anti-Sirpα (P84), anti-Ly-51 (6C3), anti-CD4 (GK1.5), anti-CD80 (16-10A1), or anti-PDGFRβ (APB5). Intracellular phosphorylated protein levels were evaluated using the FIX & PERM (fixation and permeabilization) kit (Invitrogen), according to the manufacturer's methanol-modified protocol, and stained with anti-pPDGFRβ (J24-618), anti-pIGF1R (K74-218), or anti-pErk1/2 (20A). Equal concentrations of mouse IgG1 isotype antibodies (MOPC-21) were used as negative controls for intracellular staining. Viability for in vitro studies was assessed by flow cytometry with Annexin-V and propidium iodide (PI), and DNA content was assessed using DyeCycle Violet (Invitrogen) according to manufacturer's protocols. Viable lymphoma cells were identified with anti-TCRβ (H57-957), anti-CD8a (53-6.7), anti-CD4 (RM4-5), and anti-CD3e (145-2C11). An LSRFortessa or a FACSAria II (BD Biosciences) was used for analysis and sorting, and data were analyzed with FlowJo (Treestar).

Cell Culture Media. Complete cell culture media consisted of Roswell Park Memorial Institute 1640 medium (RMPI 1640) supplemented with 1× non-essential amino acids, 55 μM β-mercaptoethanol, 2 mM GlutaMAX, 1× penicillin–streptomycin–glutamine (100 U/mL penicillin, 100 μg/mL streptomycin, 292 μg/mL glutamine), 1 mM sodium pyruvate (all from Gibco), and 10% (vol/vol) FBS (Thermo Scientific HyClone). All cultures were maintained at 37 °C in 5% CO_2.

Tumor: Stromal Cocultures. Cocultures of ex vivo lymphoma cells with bulk stroma isolated from tumors or WT thymi were prepared and cultured as previously described (20). Briefly, lymphoma cells were isolated by straining either thymic, lymph node, or splenic tumor-bearing tissue through a 40-μm filter. Stromal cells were acquired by mincing tumor-bearing or WT tissue in complete RPMI on ice. Fragments were then suspended in 10 mL of complete RPMI and vortexed. After aggregates settled for 3 min, 7 mL of supernatant was replaced with fresh RPMI to deplete lymphoma cells in solution, and the aggregates were vortexed. This process was repeated a total of three times before remaining cells were counted; 5×10^5 lymphoma cells were then cultured alone, or 2.5×10^5 lymphoma cells were cultured with 2.5×10^5 bulk stromal cells. For transwell assays, 5×10^5 lymphoma cells were seeded in the upper chamber of a 0.4-μm transwell insert dish (Corning Incorporated Costar), and 5×10^5 cells were seeded in the lower chambers; when both lymphoma cells and thymic tumor stromal cells were present in the lower chambers, they were mixed at a 1:1 ratio with 2.5×10^5 cells each.

For cocultures of tumor cells with FACS-sorted thymic stromal subsets, 2×10^6 T-ALL cells were cultured with sorted stromal subsets (5×10^5 All Stroma, 5×10^5 depleted populations, 2.5×10^5 sorted myeloid, 1×10^5 sorted DCs, or 1×10^5 sorted $CD11c^-CD11b^+$ cells) in 1 mL of RPMI in 48-well plates.

Enriched DCs from tumors and WT tissue were isolated from tissue using biotinylated anti-CD11c (N418) and streptavidin microbeads with MACS columns (Miltenyi Biotech) according to the manufacturer's instructions. Myeloid cells were further depleted using biotinylated anti-CD11b (M1/70), as indicated; 2×10^6 lymphoma cells were cultured alone or with 1×10^5 DCs. DC purities were determined by flow cytometry using anti-biotin (Bio3-18E7), anti-Sirpα (P84), and anti-I-A/I-E (M5/114.15.2).

IGF1 ELISA. DCs were enriched from WT thymi or LN3 thymic lymphomas, as described in *Tumor: Stromal Cocultures*; 1×10^5 DCs or T-ALL cells were then plated in 250 μL in 48-well plates. Supernatants were collected after 24 h and snap frozen at −80 °C. IGF1 levels were measured using a sandwich ELISA according to the manufacturer's protocol (RayBiotech).

Inhibitor and siRNA Studies. IGF1R inhibitors picropodophyllin (EMD Millipore), tyrphostin AG-1024, and BMS-754807 (Selleckchem) were resuspended in DMSO according to the manufacturer's protocols for use in cell cultures. Equal volumes of DMSO were used as vehicle controls. For IGF1R siRNA knockdown experiments, 2×10^6 T-ALL cells with 1×10^5 DCs were cultured for 24 h in 0.4 mL and then treated with 2.5 μM Accell IGF1R-targeted SMARTpool siRNA or Accell Nontargeting Pool siRNA for an additional 6 d according to the manufacturer's protocol (Dharmacon).

Two-Photon Fluorescence Microscopy. Two-photon imaging of thymocytes or tumor cells migrating within thymic slices was carried out as described previously (27). Briefly, 400-μm thymic slices from CD11c-EYFP transgenic mice (28) were prepared using a vibratome (Leica), and WT thymocytes or LN3 tumor cells, labeled with CellTracker CMTPX Red or CMF2HC Blue (Invitrogen), were incubated with thymic slices for 1–4 h at 37 °C in 5% CO_2. Images were acquired every 15 s, through a depth of 40 μm, in 5-μm intervals with an Ultima IV microscope (Prairie) equipped with two MaiTai lasers (Spectra-Physics) and PrairieView acquisition software. Excitation wavelengths of 840 nm, or 740 and 900 nm for three-color imaging, were used; 480/40, 535/50, and 607/45 bandpass filters (Chroma Technology) were used for detection of CMF2HC, EYFP, and CMTPX fluorescence, respectively. Imaris software version 7.6 (Bitplane) was used for cell tracking. Cellular interactions were scored when the distance between cell surfaces was less than 3 μm. The percentage of time contacting DCs equals the percentage of all tracked time points in which a cell contacts a DC. Dwell time equals the total time during which thymocytes contact DCs in consecutive time points.

Global Gene Expression Analysis. Genome-wide expression analysis was performed on T-ALL cells and DC subsets sorted from LN3 thymic tumors using Affymetrix GeneChip Mouse Genome 430 2.0 Arrays ($n = 3$, LN3 tumor $Sirp\alpha^+$ DCs and $Sirp\alpha^-$ DCs; $n = 3$, T-ALL cells). We have previously reported expression profiling of WT thymic DCs and thymocytes (32, 60) [Gene Expression Omnibus (GEO) accession nos. GSE34723 and GSE56928]; 1 μg of total RNA from 3×10^4 sorted tumor-associated $Sirp\alpha^+$ DCs, $Sirp\alpha^-$ DCs, or T-ALL cells was amplified, labeled, and hybridized according to the manufacturer's specifications. Data were uploaded to Gene Expression Commons (32) for normalization and analysis; an in silico model containing these datasets, along with WT thymocytes and DCs from C57BL/6J mice at 6 mo of age, is available in Gene Expression Commons (https://gexc.stanford.edu/models/1118/genes); the data have also been deposited in GEO (GSE54609). For hierarchical clustering (Euclidean complete with average linkage), we used R package Easy Microarray data Analysis (EMA) (61) to cluster thymic 6-mo WT or tumor-associated LN3 DC subsets, WT $CD4^+CD8^-$ thymocytes, and the following peripheral myeloid subsets: common myeloid progenitors (CMP), $CD8^+$ DCs, $CD8^-$ DCs, plasmacytoid DCs (pDCs), monocytes, BM macrophages (BM Mac.), and peritoneal macrophages (Mac.). Reference datasets were downloaded from GEO (accession nos. GSE10246 and GSE34723) (31, 32) and normalized with thymic DC datasets using GC robust multi-array average (GCRMA). GO analyses were carried out using the database for annotation, visualization, and integrated discovery (DAVID) Bioinformatics Database (62).

Human T-ALL gene expression datasets were generated with Affymetrix U133A chips and comprised ETP and non-ETP cases. CEL files were kindly provided by Charles Mullighan from cases at St. Jude Children's Research Hospital, Memphis, TN, and have been previously described (GEO accession no. GSE33315) (25, 33). Microarray data were normalized using the Robust MultiChip Averaging (RMA) algorithm (58), as implemented in the Bioconductor package Affy. For pairwise group comparisons, we used *t* test in the Limma package (59) in Bioconductor to identify differentially expressed probe sets between ETP and non-ETP cases under comparison. The implementation of *t* test in Limma uses an empirical Bayes method to moderate the SEs of the estimated log-fold changes, and *P* values were corrected using the false-discovery method.

Statistical Analysis. Statistical significance was determined with one sample, paired and unpaired Student's *t* tests using GraphPad Prism software (GraphPad).

ACKNOWLEDGMENTS. We thank Coby Tran for assistance with immunostaining, Ellen R. Richie for helpful discussions, and Michele Redell for her advice and expertise in human hematologic malignancies. We also thank the staff at The University of Texas at Austin Animal Facilities. This work was supported by Recruitment Award R1003 from the Cancer Prevention and Research Institute of Texas (to L.I.R.E.) and by the Intramural Research Program of the NIH (PEL: Project number: 1ZIAHD001803-22). T.A.T. was supported by Postdoctoral Fellowship PF-14-216-01-TBG from the American Cancer Society.

1. Van Vlierberghe P, Ferrando A (2012) The molecular basis of T cell acute lymphoblastic leukemia. *J Clin Invest* 122(10):3398–3406.
2. Egeblad M, Nakasone ES, Werb Z (2010) Tumors as organs: Complex tissues that interface with the entire organism. *Dev Cell* 18(6):884–901.
3. Bhowmick NA, Neilson EG, Moses HL (2004) Stromal fibroblasts in cancer initiation and progression. *Nature* 432(7015):332–337.
4. Lawrence T, Natoli G (2011) Transcriptional regulation of macrophage polarization: Enabling diversity with identity. *Nat Rev Immunol* 11(11):750–761.
5. Lewis CE, Leek R, Harris A, McGee JO (1995) Cytokine regulation of angiogenesis in breast cancer: The role of tumor-associated macrophages. *J Leukoc Biol* 57(5): 747–751.
6. Cieslewicz M, et al. (2013) Targeted delivery of proapoptotic peptides to tumor-associated macrophages improves survival. *Proc Natl Acad Sci USA* 110(40):15919–15924.
7. Zeisberger SM, et al. (2006) Clodronate-liposome-mediated depletion of tumour-associated macrophages: A new and highly effective antiangiogenic therapy approach. *Br J Cancer* 95(3):272–281.
8. Kimura YN, et al. (2007) Inflammatory stimuli from macrophages and cancer cells synergistically promote tumor growth and angiogenesis. *Cancer Sci* 98(12):2009–2018.
9. Gabrilovich D (2004) Mechanisms and functional significance of tumour-induced dendritic-cell defects. *Nat Rev Immunol* 4(12):941–952.
10. Armstrong F, et al. (2009) NOTCH is a key regulator of human T-cell acute leukemia initiating cell activity. *Blood* 113(8):1730–1740.
11. Love PE, Bhandoola A (2011) Signal integration and crosstalk during thymocyte migration and emigration. *Nat Rev Immunol* 11(7):469–477.
12. Hu Z, Lancaster JN, Ehrlich LIR (2015) The Contribution of Chemokines and Migration to the Induction of Central Tolerance in the Thymus. *Front Immunol* 6:398.
13. Shitara S, et al. (2013) IL-7 produced by thymic epithelial cells plays a major role in the development of thymocytes and TCR$\gamma\delta$+ intraepithelial lymphocytes. *J Immunol* 190(12):6173–6179.
14. Koch U, et al. (2008) Delta-like 4 is the essential, nonredundant ligand for Notch1 during thymic T cell lineage commitment. *J Exp Med* 205(11):2515–2523.
15. Hozumi K, et al. (2008) Delta-like 4 is indispensable in thymic environment specific for T cell development. *J Exp Med* 205(11):2507–2513.
16. Silva A, et al. (2011) IL-7 contributes to the progression of human T-cell acute lymphoblastic leukemias. *Cancer Res* 71(14):4780–4789.
17. Scupoli MT, et al. (2007) Interleukin 7 requirement for survival of T-cell acute lymphoblastic leukemia and human thymocytes on bone marrow stroma. *Haematologica* 92(2):264–266.
18. Scupoli MT, et al. (2003) Thymic epithelial cells promote survival of human T-cell acute lymphoblastic leukemia blasts: The role of interleukin-7. *Haematologica* 88(11): 1229–1237.
19. Gachet S, et al. (2013) Leukemia-initiating cell activity requires calcineurin in T-cell acute lymphoblastic leukemia. *Leukemia* 27(12):2289–2300.
20. Richie ER, Walker DA (2000) Production and characterization of immature murine T-lymphoma cell lines. *Methods Mol Biol* 134:177–184.
21. Serwold T, et al. (2010) T-cell receptor-driven lymphomagenesis in mice derived from a reprogrammed T cell. *Proc Natl Acad Sci USA* 107(44):18939–18943.
22. Weng AP, et al. (2004) Activating mutations of NOTCH1 in human T cell acute lymphoblastic leukemia. *Science* 306(5694):269–271.
23. Davey GM, Tucek-Szabo CL, Boyd RL (1996) Characterization of the AKR thymic microenvironment and its influence on thymocyte differentiation and lymphoma development. *Leuk Res* 20(10):853–866.
24. Li J, Park J, Foss D, Goldschneider I (2009) Thymus-homing peripheral dendritic cells constitute two of the three major subsets of dendritic cells in the steady-state thymus. *J Exp Med* 206(3):607–622.
25. Smith S, et al. (2014) LIM domain only-2 (LMO2) induces T-cell leukemia by two distinct pathways. *PLoS One* 9(1):e85883.
26. Lutzny G, et al. (2013) Protein kinase c-β-dependent activation of NF-κB in stromal cells is indispensable for the survival of chronic lymphocytic leukemia B cells in vivo. *Cancer Cell* 23(1):77–92.
27. Ehrlich LIR, Oh DY, Weissman IL, Lewis RS (2009) Differential contribution of chemotaxis and substrate restriction to segregation of immature and mature thymocytes. *Immunity* 31(6):986–998.
28. Lindquist RL, et al. (2004) Visualizing dendritic cell networks in vivo. *Nat Immunol* 5(12):1243–1250.
29. van de Ven R, Lindenberg JJ, Oosterhoff D, de Gruijl TD (2013) Dendritic Cell Plasticity in Tumor-Conditioned Skin: CD14(+) Cells at the Cross-Roads of Immune Activation and Suppression. *Front Immunol* 4:403.
30. Meredith MM, et al. (2012) Expression of the zinc finger transcription factor zDC (Zbtb46, Btbd4) defines the classical dendritic cell lineage. *J Exp Med* 209(6):1153–1165.
31. Lattin JE, et al. (2008) Expression analysis of G Protein-Coupled Receptors in mouse macrophages. *Immunome Res* 4(1):5.
32. Seita J, et al. (2012) Gene Expression Commons: An open platform for absolute gene expression profiling. *PLoS One* 7(7):e40321.
33. Zhang J, et al. (2012) The genetic basis of early T-cell precursor acute lymphoblastic leukaemia. *Nature* 481(7380):157–163.
34. Coustan-Smith E, et al. (2009) Early T-cell precursor leukaemia: A subtype of very high-risk acute lymphoblastic leukaemia. *Lancet Oncol* 10(2):147–156.
35. Medyouf H, et al. (2011) High-level IGF1R expression is required for leukemia-initiating cell activity in T-ALL and is supported by Notch signaling. *J Exp Med* 208(9): 1809–1822.
36. Cao Y (2013) Multifarious functions of PDGFs and PDGFRs in tumor growth and metastasis. *Trends Mol Med* 19(8):460–473.
37. Sebolt-Leopold JS, Herrera R (2004) Targeting the mitogen-activated protein kinase cascade to treat cancer. *Nat Rev Cancer* 4(12):937–947.
38. Brocardo MG, et al. (2001) Early effects of insulin-like growth factor-1 in activated human T lymphocytes. *J Leukoc Biol* 70(2):297–305.
39. Pollak MN, Schernhammer ES, Hankinson SE (2004) Insulin-like growth factors and neoplasia. *Nat Rev Cancer* 4(7):505–518.
40. Yaktapour N, et al. (2013) Insulin-like growth factor-1 receptor (IGF1R) as a novel target in chronic lymphocytic leukemia. *Blood* 122(9):1621–1633.
41. Shi P, et al. (2009) IGF-IR tyrosine kinase interacts with NPM-ALK oncogene to induce survival of T-cell ALK+ anaplastic large-cell lymphoma cells. *Blood* 114(2):360–370.
42. Párrizas M, Gazit A, Levitzki A, Wertheimer E, LeRoith D (1997) Specific inhibition of insulin-like growth factor-1 and insulin receptor tyrosine kinase activity and biological function by tyrphostins. *Endocrinology* 138(4):1427–1433.
43. Girnita A, et al. (2004) Cyclolignans as inhibitors of the insulin-like growth factor-1 receptor and malignant cell growth. *Cancer Res* 64(1):236–242.
44. Carboni JM, et al. (2009) BMS-754807, a small molecule inhibitor of insulin-like growth factor-1R/IR. *Mol Cancer Ther* 8(12):3341–3349.
45. Vasilcanu D, et al. (2004) The cyclolignan PPP induces activation loop-specific inhibition of tyrosine phosphorylation of the insulin-like growth factor-1 receptor. Link to the phosphatidyl inositol-3 kinase/Akt apoptotic pathway. *Oncogene* 23(47): 7854–7862.
46. Deutsch E, et al. (2004) Tyrosine kinase inhibitor AG1024 exerts antileukaemic effects on STI571-resistant Bcr-Abl expressing cells and decreases AKT phosphorylation. *Br J Cancer* 91(9):1735–1741.
47. Berger CL, et al. (2002) The growth of cutaneous T-cell lymphoma is stimulated by immature dendritic cells. *Blood* 99(8):2929–2939.
48. Trimarchi T, et al. (2014) Genome-wide mapping and characterization of Notch-regulated long noncoding RNAs in acute leukemia. *Cell* 158(3):593–606.
49. Weroha SJ, Haluska P (2008) IGF-1 receptor inhibitors in clinical trials–early lessons. *J Mammary Gland Biol Neoplasia* 13(4):471–483.
50. Loke P, et al. (2002) IL-4 dependent alternatively-activated macrophages have a distinctive in vivo gene expression phenotype. *BMC Immunol* 3:7.
51. Raes G, et al. (2002) Differential expression of FIZZ1 and Ym1 in alternatively versus classically activated macrophages. *J Leukoc Biol* 71(4):597–602.
52. Komohara Y, et al. (2013) Clinical significance of CD163$^+$ tumor-associated macrophages in patients with adult T-cell leukemia/lymphoma. *Cancer Sci* 104(7):945–951.
53. Piccaluga PP, et al. (2005) Expression of platelet-derived growth factor receptor alpha in peripheral T-cell lymphoma not otherwise specified. *Lancet Oncol* 6(6):440.
54. Terada T (2012) TDT (-), KIT (+), CD34 (+), CD99 (+) precursor T lymphoblastic leukemia/lymphoma. *Int J Clin Exp Pathol* 5(2):167–170.
55. Laimer D, et al. (2012) PDGFR blockade is a rational and effective therapy for NPM-ALK-driven lymphomas. *Nat Med* 18(11):1699–1704.
56. Huang Y, et al. (2010) Gene expression profiling identifies emerging oncogenic pathways operating in extranodal NK/T-cell lymphoma, nasal type. *Blood* 115(6):1226–1237.
57. O'Neil J, et al. (2006) Activating Notch1 mutations in mouse models of T-ALL. *Blood* 107(2):781–785.
58. Weckx S, et al. (2005) novoSNP, a novel computational tool for sequence variation discovery. *Genome Res* 15(3):436–442.
59. Gray DHD, et al. (2008) Unbiased analysis, enrichment and purification of thymic stromal cells. *J Immunol Methods* 329(1-2):56–66.
60. Ki S, et al. (2014) Global transcriptional profiling reveals distinct functions of thymic stromal subsets and age-related changes during thymic involution. *Cell Reports* 9(1): 402–415.
61. Servant N, et al. (2010) EMA - A R package for Easy Microarray data analysis. *BMC Res Notes* 3:277.
62. Dennis G, Jr, et al. (2003) DAVID: Database for Annotation, Visualization, and Integrated Discovery. *Genome Biol* 4(5):P3.